Control Entropy identifies differential changes in complexity of walking and running gait patterns with increasing speed in highly trained runners

Stephen J. McGregor[1], Michael A. Busa[1], Joseph Skufca[3], James A. Yaggie[2], Erik M. Bollt[3]

[1]Applied Physiology Laboratory, Eastern Michigan University, [2]School of Physical Therapy, Findlay University, [3] Dept of Mathematics & Computer Science, Clarkson University

Abstract

Regularity statistics have been previously applied to walking gait measures in the hope of gaining insight into the complexity of gait under different conditions and in different populations. Traditional regularity statistics are subject to the requirement of stationarity, a limitation for examining changes in complexity under dynamic conditions such as exhaustive exercise. Using a novel measure, Control Entropy (CE), applied to triaxial continuous acceloreometry, we report changes in complexity of walking and running during increasing speeds up to exhaustion in highly trained runners. We further apply Karhunen-Loeve (K-L) analysis in a new and novel way to the patterns of CE responses in each of the three axes to identify dominant modes of CE responses in the vertical, mediolateral and anterior/posterior planes. The differential CE responses observed between the different axes in this select population may provide insight into the constraints of walking and running that can serve as benchmark comparisons for healthy untrained, and clinical populations. This represents a first report of a regularity status of running in highly trained subjects.

Lead Paragraph

Previous investigations have used regularity statistics, applied to walking gait measures, in the hope of gaining insight into the complexity of gait and factors that affect it. Most regularity statistics, though, are subject to stationarity, and this limits their usefulness for examining changes in complexity under dynamic conditions like running, and in particular, exhaustive running. Using a novel measure, Control Entropy (CE), applied to triaxial continuous acceloreometry, we report changes in complexity of walking and running during increasing speeds up to exhaustion in highly trained runners. Particular

properties of CE allow us to interpret control constraints of the physiological system as a feedback control plant, and changes therein become of particular biological interest. We further apply Karhunen-Loeve (K-L) analysis in a new and novel way to the patterns of CE responses in each of the three axes to identify dominant modes of CE responses in the vertical, mediolateral and anterior/posterior planes. The results reported here may serve as a benchmark and provide insight into factors that affect complexity of gait in untrained or clinical populations.

Introduction

Running is a popular participation sport, with 10.5 million participants running at least 100 days/year [1]. Despite its popularity, there is little data with regard to the gait patterns of highly trained or elite runners, particularly during maximal exertion and/or fatigue. Presumably, with accumulated specific training, these individuals would develop the optimal pattern of movement for a particular activity [2, 3] . Moreover, it could be argued that not only would trained individuals find the optimal movement pattern, they would also exhibit optimal variability, though, as it has been argued that practice/training imparts both higher and lower variability [2], and it is not clear which is best for optimal performance. Further, the nature of the variability that is identified (linear vs non-linear) may impact the interpretation of the results. Regardless, by looking at the characteristics of movement patterns in highly trained athletes we may gain insight into clinical aspects of gait. Alternatively, characteristics exhibited by accomplished runners might serve as models of optimization for the development of robotic locomotion systems [4, 5].

A specific area of research interest regards the impact of fatigue on gait, important because gait patterns change under conditions of fatigue [3, 6-9], which can have ramifications for activity incurred injuries [1, 7]. There is likely a spectrum of gait changes under conditions of fatigue ranging from responses exhibited by clinical populations [10, 11] to those exhibited by highly trained athletes [6, 9], and again, the non-linear characteristics of these changes exhibited by trained athletes may provide unique understanding of “optimized” responses relative to normal or clinical populations.

In the field of non-linear dynamical systems analysis there are numerous tools that can provide valuable insight with regard to various aspects of human gait. In particular, tools from information theory, generally referred to as entropy or regularity statistics, have been applied to gait analysis [12-18]. Specifically, Approximate Entropy (AE) [13-16, 19] and more recently, Sample Entropy (SampEn) [18] have been used to investigate differences in regularity/complexity of gait as a result of perturbations and/or associated with normal and clinical populations. There are other related regularity approaches that have also been applied, but in general, a serious limitation to most

currently available regularity statistics is the requirement of stationarity [20]. Although statistics such as AE and SampEn are subject to conditions of stationarity, it has been fairly common in the literature to examine physiological conditions (including gait) under quasi-stationary, or even non-stationary conditions, an approach that may be expected to represent technical problems. That being said, it is often of interest to use non-linear approaches to examine physiological parameters, under non-stationary conditions. Therefore, to address this need for a regularity statistic that is not subject to conditions of stationarity, Bollt et al. [20] recently developed a novel tool termed Control Entropy (CE). A key property of control entropy is that it allows us to infer the control "effort" of a dynamical system which generates the signal being analyzed, and furthermore, it permits us to do so in a manner somewhat freed from the usual difficulties associated with requiring a stationary signal.

Bollt et al. have argued that CE is a tool that is generally applicable to any measurement signal [20], but, in particular, it is well suited to monitoring streaming, continuous signal that is recorded at high frequencies. This is in contrast to other commonly used regularity statistics that are typically applied to discretized samples (e.g. stride rate, HR). This characteristic could allow researchers to exploit the more robust information properties of streamed waveforms which may provide novel insight into the regularity of gait or other physiological parameters. One particular gait analysis tool that has recently become popular is the high resolution MEMS accelerometer (HRA). Accelerometers have been utilized for some time for both gait analysis [21-23], as well as the estimation of energy expenditure [24-27]. In the case of the later, the devices used have generally been "low resolution" in nature producing a discretized count that represents activity level, as opposed to an actual measured waveform that putatively provides more information. In the former approach, gait analysis, HRA have been used to describe characteristics of gait patterns with the objective typically to collect information in less restrictive environment imposed by a typical gait laboratory.

Recently, we have shown [28] that data obtained from high resolution accelerometers exhibit strong linear relationships to oxygen consumption (VO_2) in trained runners. Since VO_2 is an indirect measure of metabolic power, the objective of this study was to use CE analysis of continuous HRA signal obtained over a range of speeds in highly trained runners during treadmill locomotion in an effort to gain insight into the control constraints that are present in this population. The range of speeds used would encompass constrained walking, unstressed walking/running, and exhaustive running. It was anticipated that changes in CE of HRA would be reflective of the changes in constraints imposed on the individuals and this would help provide a better understanding of the changing constraints under non-stationary conditions in fit,

highly trained individuals, which could serve as baseline comparisons for other less fit/trained populations.

Methods

Subjects

Seven male NCAA Intercollegiate Division 1 runners (Table 1) gave written informed consent to take part in this study. All procedures were approved by the local Human Subjects Review Board and performed in compliance with Eastern Michigan University.

Table 1: Physical Characteristics of subjects (N=7)			
	Mean	**SD**	**Range**
BM (kg)	65.5	5.7	58.2-75
Height (cm)	181.8	4.1	175.3-188.0
Age (yr)	21.4	1.7	19-24
VO_{2peak} (mL/kg/min)	70.1	6.2	60-79
Maximal Aerobic Speed (km/h)	22.1	0.5	22-24
Maximal Speed (km/h)	21.4	0.9	20-22

Table 1: Values are mean ± SD and range. BM, body mass. VO_{2peak}, peak oxygen uptake.

Experimental Design

Subjects completed two continuous, incremental exercise tests on a motorized treadmill (True ZX-9, St. Louis, MO) with at least 6 days separating each trial. Exercise tests were performed to volitional exhaustion while high resolution triaxial accelerometry (HRA) and open circuit spirometry was collected to determine relationships between metabolic parameters (e.g. Ve, VO_2, VCO_2) HRA, walking and running speed which are presented elsewhere. The subjects reported to the laboratory on the day of testing after having refrained from strenuous exercise, alcohol, and caffeine for 24 hours prior to the day of testing and having fasted for 3 hr.

Incremental exercise tests to volitional exhaustion

In each of the two tests, subjects stood for 2 min before walking to establish a baseline measure for CE determination. At two min, they began walking at 2km/h and speed was increased 2km/h every two minutes until volitional exhaustion. The treadmill grade was held constant at 1% to simulate normal over-ground walking/running. During tests, metabolic data was collected on a breath-by-breath basis using portable open circuit spirometry (Jaeger Oxycon Mobile, CA). VO_{2max} was determined as the highest 30s average of the test. From this maximal aerobic speed (lowest speed eliciting VO_{2max}) and maximal speed (maximal speed attained before exhaustion) were determined.

Metabolic Measurements

Indirect calorimetry was used to collect breath-by-breath measurements of VO_2 and VCO_2 using electrochemical oxygen measuring cell (SBx) in an Oxycon Mobile (Cardinal Health, OH) and averaged over 5 sec. Heart rate was collected continuously via telemetry using a Polar coded transmitter belt (Polar t-31, Polar Electro, Oulu, Finland). The oxygen and carbon dioxide sensors were calibrated prior to each test for: ambient conditions (temperature and barometric pressure), volume and gas content against precision analyzed gas mixtures.

Accelerometry

The HRA device consisted of a triaxial MEMS accelerometer model ADXL210 (G-link Wireless Accelerometer Node ± 10g, Microstrain, Inc., VT). The device was mounted to a semi-rigid strap and placed, anatomically, at the intersection of the sagittal and axial planes on the posterior side of the body in line with the top of the iliac crest in order to approximate the subject's center of mass [29]. It was additionally secured with elastic tape in order to remove extraneous movement of the device not associated with locomotion. Acceleration in g's was streamed in real time using telemetry to a base station at a frequency of 625 Hz.

Linear Data Analysis

Raw accelerometry signal (in g's) was saved in Agilelink software (Microstrain, VT) and exported to Signal Express software (Labview, TX) in ASCII format. The RES value was calculated using the usual Euclidean norm,

$$RES_{xyz}^2 = (ix)^2 + (jy)^2 + (kz)^2$$

where x, y and z equal the VERT, M/L and Anterior/Posterior axes, respectively.

For determination of RMS of acceleration signal in relation to speed, full length files were parsed into 1 min segments, and the last one minute of each treadmill stage was used to calculate Root Mean Square (RMS) value using Signal Express for each axis (e.g. vertical (VERT), mediolateral (M/L), anterior/posterior (A/P), and Resultant (RES). The 1 minute RMS of acceleration in each axis were compared to speed of each corresponding stage. Comparisons were made using a linear regression curve fit (SPSS, IL; α=0.05).

Non-linear Data Analysis

We shall adapt a new tool from dynamical systems theory, namely control entropy (CE) and a second tool from statistical theory of spatiotemporal systems, namely the Karhunen-Loeve (K-L) transform, for classifying group responses. Many dynamical systems tools associated within applied measurable dynamics [30] have been adapted to classify time series from experimental sources, including those from biological sources. In many biological applications, they have been used to distinguish "healthy" from "unhealthy" biological signals. However, two key issues complicate

otherwise would be simple but popular quantifiers like Lyapunov exponents or entropies. These are embedding coordinates, including dimensionality and data population on the one hand, and then partition of the phase space in the appropriate representation for the later. Regarding embedding and representation, we will only say that a finite and finitely sampled scalar time series, $\{x(t_i)\}_{i=1}^{N}$, from some experiment, numerical or physical, is presumed to have a representation as an m-dimensional dynamical system. A great deal has been written about how delay embedding coordinates using the Taken's method [31] can produce sufficient representations, and how to use such concepts to deduce appropriate and sufficient coordinates in practical computations. This literature is extensive and remains active [30, 32], and is in a sense a complementary problem to that which we wish to work here, regarding change detection, health monitoring, and gaining insight into control effort. We present methods of systems monitoring for "control effort" and health monitoring by what we call control entropy (CE). Furthermore, we discuss here a method for group analysis of responses. This group analysis is based on a variation of principle component analysis (PCA), with some registration, which may also be considered an adaptation of the K-L transform, so popular recently [33] in empirical analysis of partial differential equations.

Control Entropy

In [20] we developed a regularity statistic which we call control entropy (CE). Our goal was an entropy- like regularity statistic that can be applied against (possibly) nonstationary time series data in a way that allows insight into the (possibly) time varying parameters of the system. While there is a long well understood tradition in measurable dynamics and ergodic theory to relate concepts of informaton theory, and the Shannon entropy [34, 35],

$$SE = -\sum p_i \ln p$$

motivates, in a sense, the Renyi-entropies, following [32, 36],

$$K_q = \lim_{r\to 0}\lim_{m\to\infty}\frac{1}{1-q}\ln I_q(r), \text{ where, } I_q(r) = \sum (p_j)^q, q \geq 0,$$

where m-dimensional partitions of uniformly sized hypercubes of side r-hypercubes with relative occupancy probability p_i, although in general, one must define the supremum

over all possible partitions and their refinements. A most notable entropy for our discussion here is the Komolgorov-Sinai (KS) entropy, which is the special case K_1, often called measure theoretic entropy [37] and widely considered as a quantifier of information theoretic complexity of a dynamical system, descriptive of the rate at which the system looses precision and amplifies noise and errors. Due to difficulties in estimating K_1, one often considers the lower bounding which follows from convexity [38], K_2, which can be associated with the so-called correlation entropy [30, 39]. K_2 is often preferred in calculation regarding data sets since it can be computed more quickly and accurately by consideration of a correlation integral such as described by Theiler in [30]. In practice, in consideration of data sets sampled from empirical, analytical or experimental systems considered to be inherently dynamical systems, a good deal of attention has been paid to the approximate entropy (AE) of Pincus [40-42], (approximate entropy, also introduced as a regularity statistic), and a more recent modifcation called sample entropy (SampEn) designed to remove self matching biases inherent in ApEn. We wish to point out that the many excellent algorithms from numerical ergodic theory built into the popular package TISEAN include reliable estimators of K_2 in the spirit of [30]. The difficulty to relate such concepts to dynamical systems must consider appropriate embedding.

While in the case of a chaotic dynamical system with an invariant measure, it is suitable to discuss the full Renyi spectrum of entropies [39], it becomes less well founded for our goal problem, to identify changes in complexity of non-stationary time-series data.

We defined control entropy via correlation sums [20]. Suppose a data set $\{z_i\}_{i=1}^{N}$ to be a scalar time series from an ergodic process sampled on a uniform time grid. Let an embedding dimension m by a delay embedding [29], $v_i = (z_i, z_{i-1}, ..., z_{i-m+1})$, with unit index delay. The correlation sum is given [39],

$$C_2(\{z_i\}; m, r, T) = \frac{1}{N_{pairs}} \sum_{i=m}^{N} \sum_{j<i-T}^{N} \Theta(r - \| v_i - v_j \|_\infty$$

where Θ is the Heaviside function, r is a parameter defining a neighborhood, and $N_{pairs} = (N-m+1)(N-m-w+1)/2$ is the total number of pairs of delay vectors. Integer parameter $T \geq 1$ is a Theiler window used to mitigate effects of time correlation in the data. Let,

$$\hat{h}(\{z_i\};m,r,T) = \ln \frac{C_2(\{z_i\},m,r,T\})}{C_2(\{z_i\},m+1,r,T\})}.$$

which may be considered as a regularity measure, independent of any attempt to relate this to asymptotic and limiting values by considerations of scaling regimes. This formula lead to the development of SampEn [43, 44]. Thus, we may define,

$$SE(j+J,w,\{z_i\}_{i=1}^{n};m,r,T) = \hat{h}(\{z_i\}_{i=1+j}^{w+j};m,r,T) \text{ for } 0 \le j \le n-w,$$

where J represents time offsets. SampEn, with these arguments, represents an entropy assignment to each time window of dataset, and associated to each time instant J. From the SampEn entropy of a signal $\{z_i\}$, we define the control entropy of the signal,

$$CE(j+J,w,\{z_i\}_{i=1}^{n};m,r,T) = SE(j+J,w,\{z_i - z_{i-1}\}_{i=2}^{n};m,r,T) \text{ for } 0 \le j \le n-w,$$

in terms of first difference of the signal. We have found that symbolization adds a great deal of stability, but still has sufficient robustness and rapid convergence relative to the continuous r-neighborhood statistic. We choose a symbolized control entropy statistic,

$$CE_b(j+J,w,\{z_i\}_{i=1}^{n};m,r,T) = CE(j+J,w,\{s_i\}_{i=1}^{n};m,0.5,T) \quad (1)$$

where b denotes a symbol set. As discussed specifically in our [20], and in theoretical basis in [43, 44], the specific choice of partition, that is symbolization function converting continuous signal value, x_i into symbols s_i. In [20], we presented two major approaches, one being by signs, $b = \{-1,0,1\}$ by $s_i = sign(x_i - x_{i-1})$. The other is the SAX_n method [45] which we adopt here, where by b is chosen to consist of n symbols, and x_i is mapped to s_i according to an equipartition of Z-values from a normal model on the

data set. We shall use the SAX_n symbolization in computing CE_b as according to an entropy time series according to Eq. (1), where n will be chosen to satisfy the saturation criterion which we described in [20] – that is if measured CE_b becomes $\ln n$ at any time t, then it is assumed that n is too small and the cause is that there is overloading of symbolization, as described in detail in the theoretical work in [43, 44].

Registered Principle Component Analysis and the Karhunen Loeve Transform for Analysis of Groups of CE Time Series

Principle Component Analysis (PCA) as applied to groups of time series, especially spatiotemporal data sets as is typical in the partial differential equations literature [33, 46], has become to be known as Principle Orthogonal Decomposition (POD) as well as the Karhunen-Loeve Transform (K-L). The analysis of many time series can be cast into standard terms, and discussed by Singular Value Decomposition (SVD) [47], which we review here. Note that there are many points here will remind the reader of facial image analysis methods, so called Eigenfaces [48], which involves similar steps, namely registration of the signal, and then decomposition into principle components which are optimal across the time average population. As applied to a population of signals, such a population of CE times series, we note that this part of our analysis could and should be applied to any other entropy analysis designed to track complexity changes in time, across populations.

Considering a population of p members, each of which presents a signal, thus presenting theoretical data set, $\{z_i(t)\}_{i=1}^{p}$, which however in practice is discretely sampled in time, $\{\{z_i(t_j)\}_{j=1}^{N}\}_{i=1}^{P}$ may rather be considered as a data array, $Z_{p\times N}$,

$$Z_{i,j} = z_i(t_j).$$

While we have written this in general terms, here we shall always take each $z_i(t)$ to be the CE time series signal processed from each of the ith member sampled. Then considering demeaned data, we would denote

$$\hat{Z}_{i,j} = z_i(t_j) - \sum_j z_i(t_j), \quad (2)$$

but for comparison to common spatiotemporal analysis notation, $w(i,t) \equiv \hat{Z}_{i,t}$, where due to sampling, t is one of t_j, $1 \le j \le N$. Then, K-L eigenmodes are the eigenfunctions of the autocorrelation matrix,

$$K_{j,j'} = < \hat{Z}_{i,j} \hat{Z}_{i,j'} > = \frac{1}{P} \sum_i \hat{Z}_{i,j} \hat{Z}_{i,j'},$$

which denotes products at each time pairing t_j and $t_{j'}$, averaged across sample indexed by i, where the brackets <.> denotes integration across the sample set indexed by i. It is known by the spectral decomposition theorem [47], that the eigenfunctions of K are orthogonal, since K must be positive semidefinite, and represent an optimal basis in population average. Therefore, writing as in K-L analysis, we write,

$$w(i,t) = \sum_{n=1}^{P} a_n(i) \phi_n(t). \quad (3)$$

Here, $\phi_n(t)$ denotes the eigenfunction, which is a function of time, and $a_n(i)$ is the coefficient of projection for each sample. However, unlike the use of such a modal expression in spatiotemporal systems [46], with both time-t and space aspects, we use this expression where i-denotes the index of the members, as is more typical in POD analysis, and as used in such applications as Eigenfaces [33]. What is most relevant and special concerning this modal analysis, in contrast say to a modal expansion in terms of Fourier sines and cosines, is that the modes $\phi_n(i)$ are known to be orthogonal, and optimal in average. That is, the power spectrum is fastest decaying in time average, when compared to a power spectrum as developed by any other basis set. These statements both follow a spectral decomposition analysis [47], or alternatively by [46]. Orthogonality in time means,

$$< a_n(i) a_m(i) > = \lambda_n \delta_{nm},$$

in terms of the bracket <.> of sums averages across the sample. Here, λ_n are the eigenvalues of K; the expressionn represents the decorrelated Fourier coefficients $a_n(i)$. By consequence, projecting data Eq. (2) onto each mode $\phi_n(t)$ gives uncorrelated samples from each mode, which is a statement of statistical independence. An eigenvalue may be written,

$$\lambda_n = \frac{(\phi_n, K\phi)}{\| \phi_n \|} = <| (\phi_n, w) |^2>$$

where round parahentesis (.,.) denote an inner product with respect to integration in time, $(f(t), g(t)) = \int_0^T f(t)g(t)dt$, and <.> denotes the average across the samples. In these terms the K-L modes have been shown to also be derived by a problem of calculus of variations to optimize the projection of the data onto each successive mode [46], meaning, the power spectrum (as seen in Figures 6c, 7c, 8c, and 9c) decays faster in time average than a power spectrum would using any other basis set of functions.

We note that better power spectral decomposition, again meaning fastest decaying power spectrum, will be achieved if the time series data is registered, meaning events are shifted so as to start at the same instant. Stated simply, the data may be shifted to pairwise minimize a convolution integral,

$$z_j(t) = \arg\min_{\tau} \int z_i(t_j) z_j(t - \tau) dt$$

before resorting to demeaning (2). In practice, we take a simplified version of this registration statement.

Considering the data as statistical samples from an appropriate random sample, we may interpret the K-L analysis as descriptive as maximally decorrelated representations

of a least squares model, from which description leads to confidence limits on the model [49]. The setting in which the singular values and singular vectors lead to statistical confidence in the representation is the language of multivariate regression analysis. Said succinctly, Eq (3) can be considered to be a standard regression problem related to optimal low-rank representation of a matrix by the spectral decomposition theorem,

$$K = \sum_{n=1}^{P} \frac{1}{s_n^2} v_{(n)} \otimes v_{(n)}$$

where the singular vectors and singular values of K describe the correlation matrix K. Again this is the spectral decomposition theorem stating that K may be represented as a sorted sum of rank one projector matrices, $v_{(n)} \otimes v_{(n)}$, weighted inversely proportionally to the singular values, s_n^2 . Viewing the SVD as the solution of a least squares problem in the over determined case, the representation relates to a χ^2 distribution in the fitted parameters by treating the sample of data as an ellipsoid cloud in the parameter space, where the length of the major and minor axis of the ellipsoid are inversely proportional to each s_n^2. Equivalently, taking the data as a statistically sampled ensemble with standard assumptions regarding normally distributed i.i.d. data, SVD yields the least squares solution to a parametric fit descriptive of how each individual signal is a linear combination of the singular vectors by an equation which describes level curves of the χ^2 distribution, [49, 50],

$$\Delta\chi^2 = s_1^2(v_1 \cdot \delta a) + s_2^2(v_{21} \cdot \delta a) + \ldots + s_P^2(v_P \cdot \delta a) \quad (4)$$

where δa describes the projection of a particular data point (a new sampled experimental and processed CE time series in this case) onto the singular vectors. As such, by orthogonality, this gives a direct description of the likelihood of a new data set by inspection of the energy of the new sample in the energy spectrum tail, which describe the unlikely modes in the original representative data set.

The point here is that a fast decaying average power spectrum indicates that only a few singular vectors describe dominant modes, then if a new experimental data set is brought to bear, it can be compared to the current data set by projection onto those singular vectors basis which capture most of the energy of the original population. If

there is a large representation in the orthogonal unlikely modes, then this represents an experiment which is unlike the original data set with great confidence. Specifically interpreting Eq. (4), projections onto the few major axis and therefore the time average of the projected coefficients, when the data is tightly correlated, it is all contained within a low dimensional ellipsoid. On the other hand, any outlier data is quickly identified as outlying such an ellipsoid. Referring this statement to the running data in Figure 8, where it is already apparent in the CE time series that two members of the population are somewhat different from the rest, one greatly so, we corraborate this appearance with the time average spectral projections as shown in Figure 10.

Results

Linear characteristics of unfiltered signal

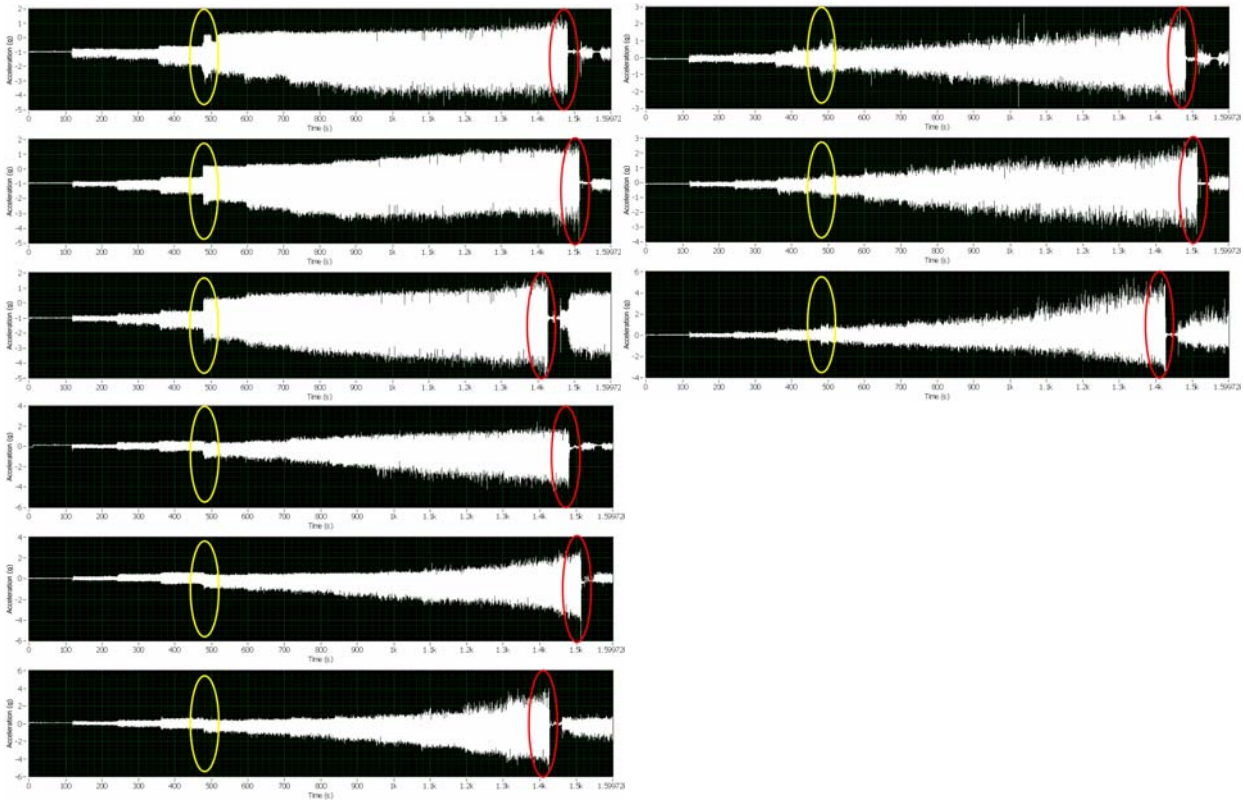

Figure1. Unfiltered accelerometry signal collected during incremental treadmill trials starting at 2 km/h (after 2 minutes of quiet standing) and increasing 2 km/h every 2 minutes until exhaustion. a) VERT b) M/L c) A/P. Yellow circles identify the walk to run transition and red circles identify exhaustion.

Unfiltered accelerometry signal of three representative subjects is presented in Figure 1. The subjects represent the best and poorest performers, as well as a middle

performer (maximum speed 24, 22 and 24 kph, respectively). It is evident that each subject transitioned from walking to running at the 8 kph stage (yellow circle) regardless of performance level. This is in agreement with previous studies (Jordan and Newell) that the preferred walk to run transition occurs at approximately 7 kph. Since the highly trained athletes in the current study walked at 6 kph, and ran at 8 kph, it appears that training status may not affect preferred walk to run transition speed on a treadmill. At the first run stage, the magnitude of accelerations in the VERT axis, both positive and negative, increased dramatically relative to the last walk stage. In the A/P axis, at the walk to run transition, there is a shift in accelerations to a negative bias, and yet the magnitude of the RMS of the accelerations in this axis remain linear with relation to speed (Figure 2c, $R = 0.94$; $p<0.001$).

Regression curve fits of acceleration to speed

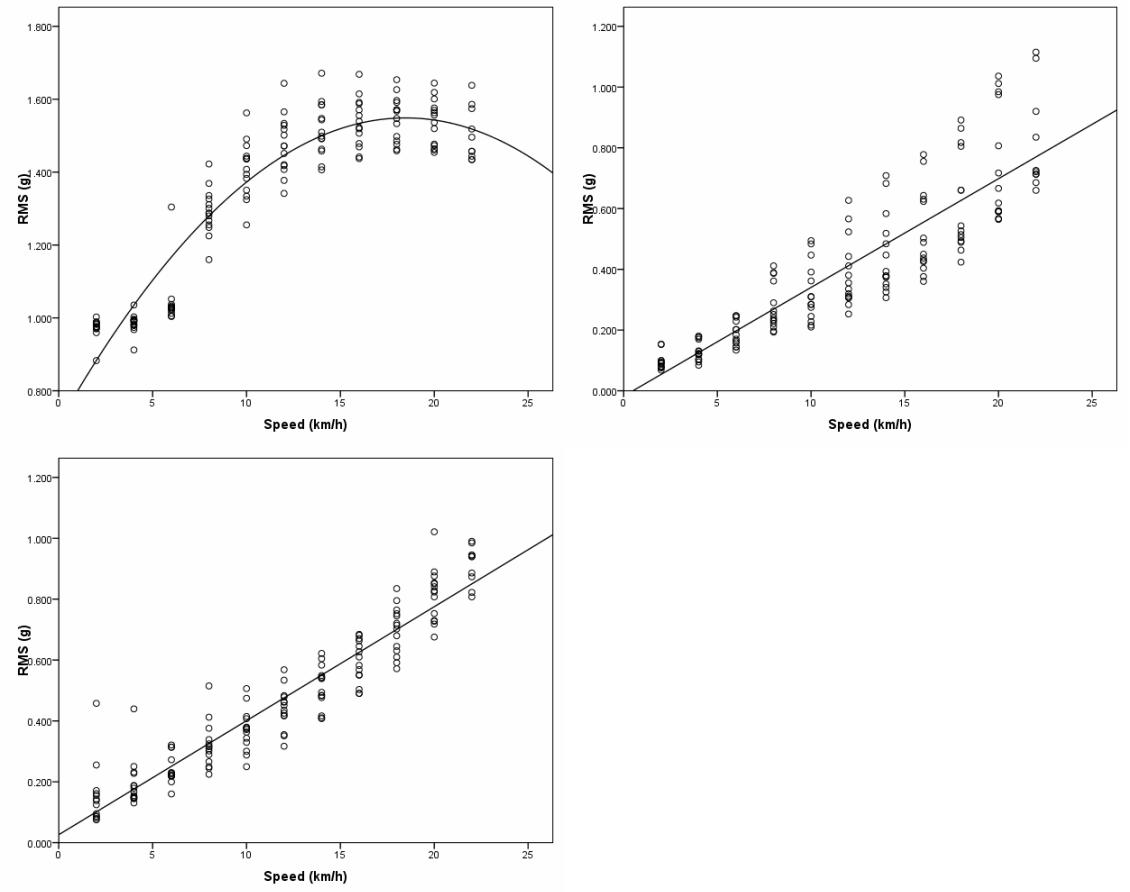

Figure 2. Curve fit regressions of 1 min RMS of accelerometry signal vs speed during incremental treadmill trials to exhaustion. The accelerations in each axis from the last 1 min of each speed were used to generate RMS of acceleration. A) VERT b) M/L c) A/P.

The VERT axis exhibited a significant quadratic fit, while M/L and A/P both exhibited linear fits (all $p<0.001$)

Regression fits of RMS values for the last 1 min of each speed are displayed in Figure 2. Both responses from the M/L and A/P axes exhibited linear relationships to speed (r = 0.88, F= 512.6; r = 0.94, F= 1201.5, respectively). In contrast, RMS of acceleration in the VERT axis was best described by a quadratic relationship to speed (r = 0.94, F = 531.0). These observations are consistent with other reports that accelerations plateau in the vertical axis during running (**REF), but, to our knowledge, a quadratic relationship has not been previously reported.

Changes in CE of accelerations in individual axes (individual responses)

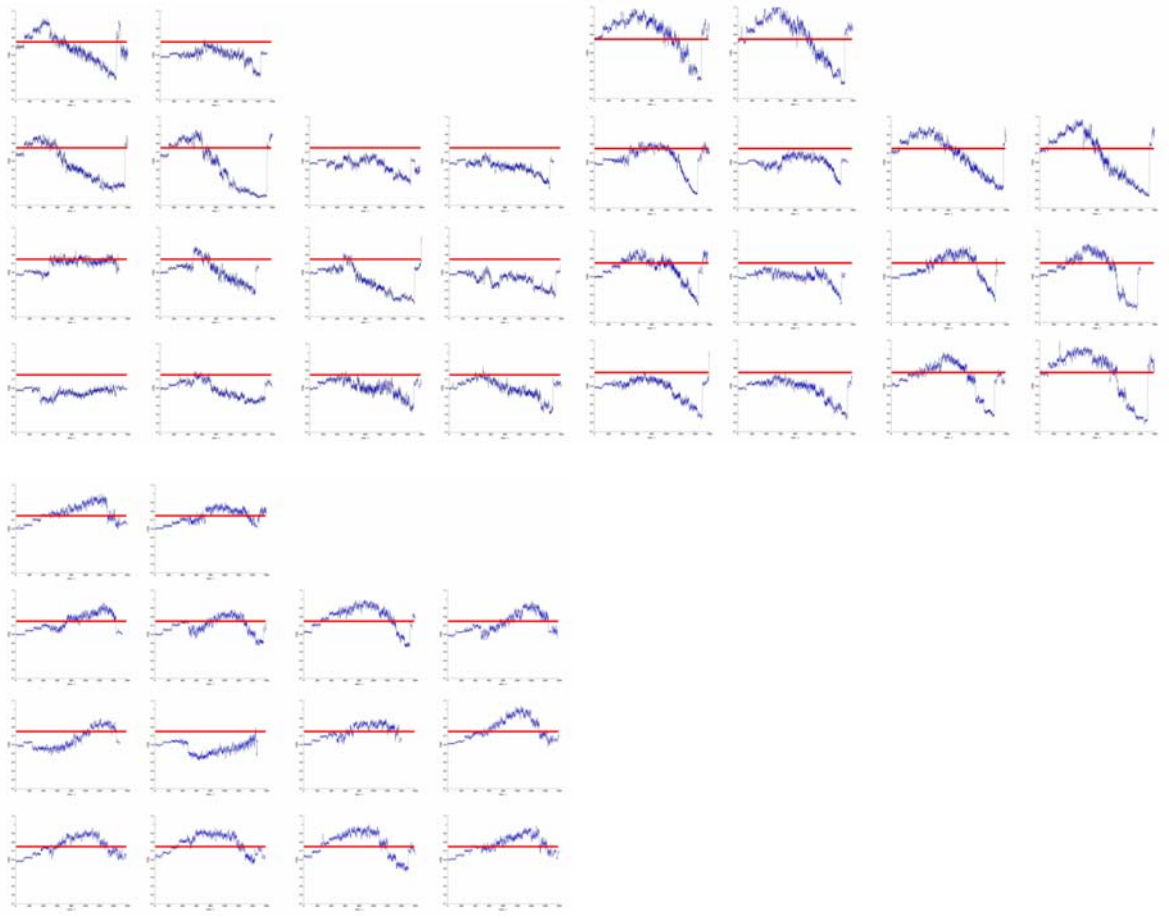

Figure 3. Plots of CE response relative to speed for individual subjects for each of two trials. (top left) = VERT, (top right) = M/L, (bottom left) = A/P. The horizontal red line corresponds to a CE = 0.75.

Individual responses of CE of accelerations in the VERT axis can be seen in Figure 3. Manually grouping data sets with similar response gives two readily apparent

aspects of the individual plots (Figure 3). First, when comparing the CE response relative to the 0.75 CE benchmark in the VERT relative to the M/L and A/P axes, it appears as though the VERT exhibits a suppressed CE. In most cases, the CE doesn't increase beyond the horizontal line corresponding to 0.75, and if it does, the peak CE occurs before the walk to run transition. In contrast, several of the individual CE plots in both the M/L and A/P axes increase above the 0.75 criterion line. In particular, CE in the A/P axis increases above the 0.75 line, and do so later than is observed in the M/L axis. These observations may provide insight in that the overall CE response in the VERT appears "suppressed", indicating higher constraints than in the other axes. This may be due to the fact that constraints due to gravity are the most significant constraints in the VERT axis and are imposed consistenly across the speed spectrum [51, 52]. The second observation here is that CE appears to reach a maximum later in the A/P compared to the VERT and M/L axes. Again, this may be indicative of the constraints unique to this particular axis [52], and may be indicative of an adaptive uncoupling [53] in this select population.

Changes in CE of accelerations in individual axes (group responses)

Results of K-L analysis of CE of accelerations for individual axes can be seen in Figures 6-8. For each axis, a dominant mode was identified (Figures 6b, 7b, and 8b) and its likelihood determined and presented as a power spectrum (Figures 6c, 7c and 8c). In the case of the VERT axis, the dominant mode contains less power relative to the collective responses. The dominant modes identified for the M/L and A/P axes contained more power (Figures 7c and 8c), with the A/P axis exhibiting the "strongest" dominant mode. When "outliers" (those with more projection component on the nondominant modes) in this response were removed, the power of the dominant mode (Figure 9b) increased substantially (Figure 9c).

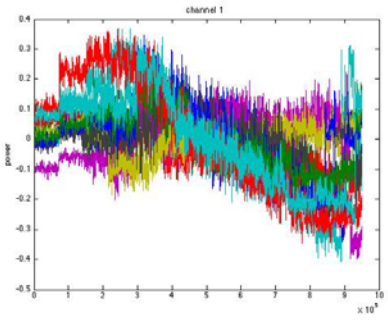

a)

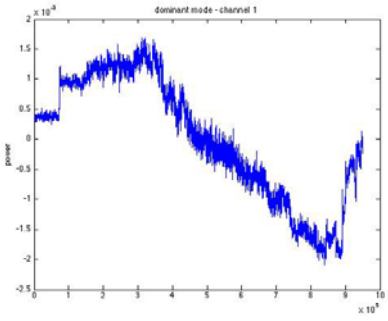

b)

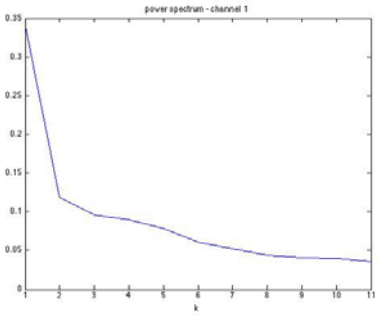

c)

Figure 6. Karhunen-Loeve (K-L) analysis: CE of accelerations in the VERT axis. a) K-L analysis b) Dominant Mode c) power spectrum

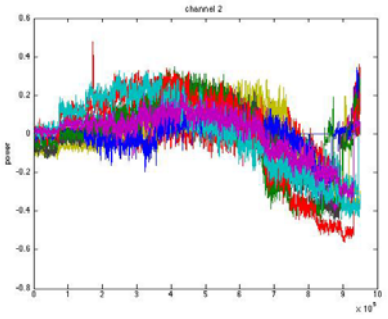

a)

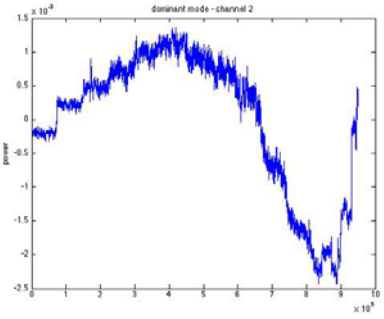

b)

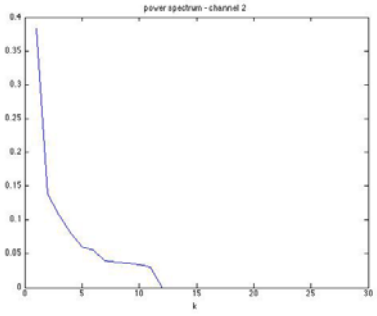

c)

Figure 7. Karhunen-Loeve (K-L) analysis: CE of accelerations in the M/L axis. a) K-L analysis b) Dominant Mode c) power spectrum

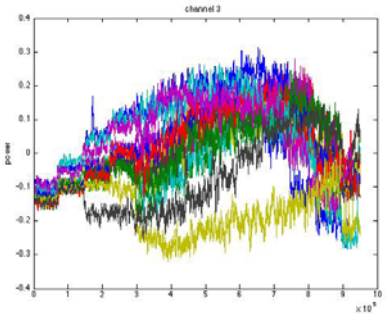

a)

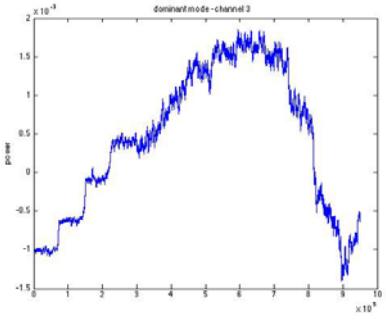

b)

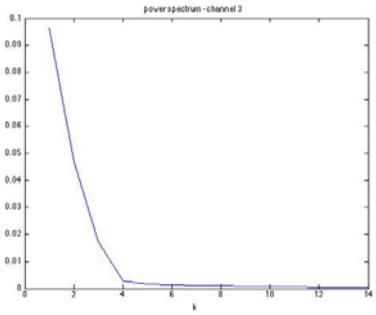

c)

Figure 8. Karhunen-Loeve (K-L) analysis: CE of accelerations in the A/P axis. a) K-L analysis b) dominant mode c) power spectrum

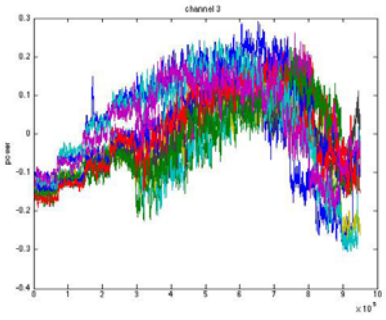

a)

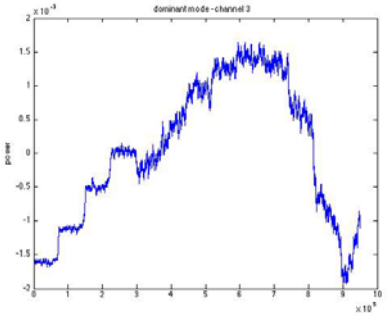

b)

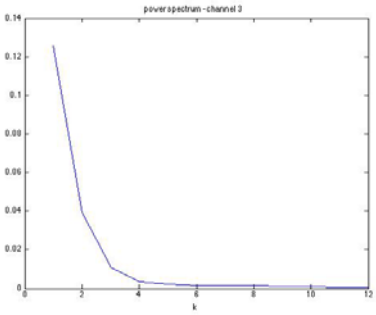

c)

Figure 9. Karhunen-Loeve (K-L) analysis: CE of accelerations in the A/P axis with outliers removed. a) K-L analysis b) Dominant Mode c) power spectrum

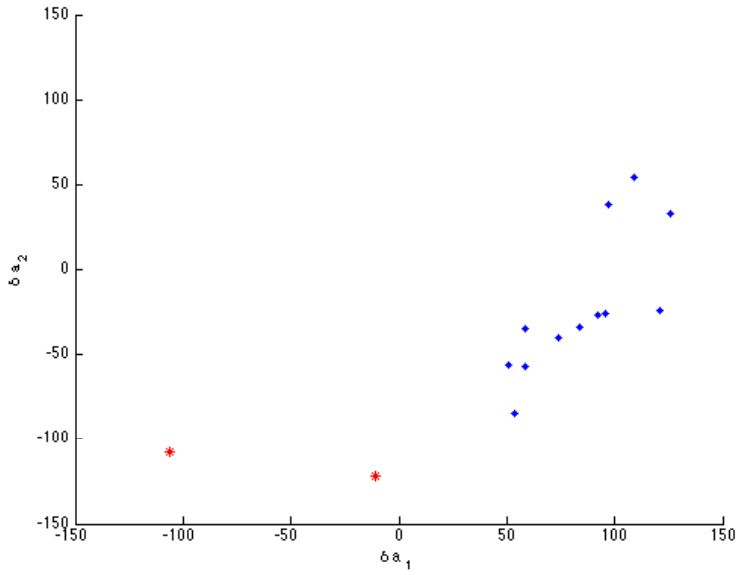

Figure 10. A projection of the demeaned CE time series of the population shown in raw form in Figure 8 onto the dominant singular vectors, v_1 and v_2, quickly identifies outlier members of the population, in this case, one significant outlier – in agreement with the two apparent outliers in Figure 8, and then furthermore that the rest of the data is tightly correlated.

Discussion

In the current study we report changes in complexity of HRA in highly trained runners over a wide range of running speeds that encompassed walking, the walk/run transition, running and volitional exhaustion. Further, signals from 3 axes were collected from the same point in space, at the approximate center of mass during locomotion, and yet, distinct differences in complexity and patterns of complexity were observed between individual axes, as well as between individuals. Finally, we demonstrate how K-L analysis can be applied to CE results to identify predominant patterns of complexity changes in these data.

Technical considerations

Two unique technical aspects of this study were the nature of the subjects utilized and the signal analyzed for changes in complexity related to the control input. It is not uncommon to use highly trained/fit subjects to present extreme examples of

optimized systems as a point of reference and contrast to sick or diseased systems and in some cases, this approach been used in both human and animal models to add insight and understanding to the nature of diseased states [54-58]. Within the context of gait analysis though, there is not an extensive literature in this regard. Specifically in the current study in reference to walking/running, it is well established that although highly trained/elite runners are certainly highly fit, and have excellent aerobic capacity, there are also biomechanical/structural characteristics that make good runners better at the task than equally fit non-runners [59-63]. Therefore, this work was intended to provide a benchmark for those who have optimized the aspects of running that will serve as a comparison to other populations in future work. In fact, several of the subjects in this study exhibited aerobic capacity (VO2max) that would be comparable to some recreational runners (e.g. VO2max ~ 60 ml/kg/min), and will serve as ideal comparators to fit, running specific non-trained populations. This will hopefully provide insight into the changes in complexity observed in optimized vs non-optimized systems with regard to running.

Typically, regularity statistics are applied to discretized or downsampled measures (e.g. heart rate, stride rate, ventilatory rate, center of posture). In contrast, in the current study, we used CE applied to the continuous, raw signal from HRA. To address the technical aspect of complexity analysis of continuous signal compared to discretized samples, it has been argued that stride rate, for example, is the “final output” of the neuromuscular control system [64]. In some sense this may be true, but it could be argued that more information is contained in the continuous signal (e.g. frequency, amplitude, direction) of a measure such as acceleration. This is evidenced by the results of the present work in which differences in complexity between different axes of movement are discernible (Figures 6-9). This phenomenon would not be observable if examining the entropy of a discrete measure such as stride rate. Further, filtering can influence the characteristics of waveform patterns, which makes this approach undesirable if avoidable. We have shown that i.i.d. noise does not adversely affect the CE analysis [20], which facilitates the use of continuous, unfiltered signal. If we compare the results of current study to previous studies that have examined changes in entropy during walking or running, but it should also be cautioned that due to the technical differences in the parameter analyzed and the nature of the statistics (e.g. partitions, embedding, etc.), differences may exist between previous studies and the current study with regard to changes in complexity. These differences may be valid despite appearing contradictory.

Changes in Control Entropy relative to walking speed

K-L analysis was performed with the purpose of identifying common CE responses and generalizing them to the population utilized for this study. In doing so,

for each axis a “dominant mode” was identified which exemplified the most likely common CE response for each axis. Therefore, for purposes of generalization we will refer to the dominant mode as exemplars of a given response, and present caveats and exceptions where necessary.

In the VERT axis, during walking at increasing speeds, the dominant K-L mode (Figure 6b) exhibited an increasing CE until the first run stage (8 kph). It should be noted though that the power of the dominant mode in the VERT axis was not strong (Figure 6c) and other moderately strong responses were observed (Figure 3, Figure 6a). This is in contrast to the M/L and A/P axes both of which exhibited more consistent CE responses. Both of the dominant modes in these axes (Figures 7b and 8b) exhibited increasing CE while walking speeds increased, and the power of these modes (Figures 7c and 8c) indicated these were the most common responses.

How can these changes in complexity during increasing walking speeds be interpreted? It has been proposed that CE can be viewed as a measure of system constraint [20]. In young, healthy humans, preferred walking speed is approximately 4 kph (1.2 m/s) [65] and it may be that CE increases during the first 3 stages during walking as a result of reduced constraint as the individuals reach preferred gait speed. In the A/P axis though, this is unlikely as CE continues to increase in the dominant mode during run phase (discussed later). Further, the inconsistent response in the VERT axis is difficult to interpret as well. Buzzi and Ulrich [13] reported decreasing AE with increasing walking speed in both healthy and comparably aged youth with Down Syndrome (DS). To our knowledge, there have been no other reports of changes in regularity measures such as AE or SampEn with changes in walking speed. It should be noted though that the same authors [13] reported decreased Lyapanov exponent (LyE) of joint segments with increasing walking speed. Further the DS subjects exhibited significantly higher LyE than controls, which the authors claimed indicated DS exhibited increased instability of gait relative to controls, but instability of gait decreased with increasing speed in both groups. This is in contrast to England and Granata [66] who recently reported increasing maximum finite-time LyE of various joint angles with increasing walking speed. This included speeds beyond preferred walking speed and preferred walk-run transition. The authors interpreted these observations as indicating increased instability of gait as walking speeds increased.

Changes in Control Entropy relative to running speed

In the VERT axis, after the walk-run transition, during running at increasing speeds, the dominant K-L mode (Figure 6b) exhibited a decreasing CE until exhaustion

where the CE was lower than the starting point both standing and during the initial walk stage (2 kph). As was noted in the previous section, the power of the dominant mode in the VERT axis was not strong (Figure 6c) and therefore a generalization regarding CE of acceleration in the VERT axis during running is difficult to make. As we point out in "Changes in CE of accelerations in individual axes (individual responses)" in reference to Figure 3, when examining individual plots, CE does not appear to rise to the same extent in the VERT axis relative to the other two axes. Further, the "peak" CE response appears to occur sooner, during the walking phase, relative to the other two axes. In several cases, the CE increases in the A/P well into the run phase and generally peaks latest in this axis. Group analysis using the K-L method confirmed this observation. In the M/L and A/P axes both of which exhibited more consistent CE responses than the VERT axis, the dominant modes in these axes (Figures 7b and 8b) exhibited decreasing CE while running speeds increased, and, again, the power of these modes (Figures 7c and 8c) indicated these were the most typical responses for each axis.

In general, with regard to changes in complexity with changes in speed during running, there are few direct comparisons in the literature because, to our knowledge, no other investigators have examined changes in gait characteristics during running using non-linear regularity statistics. By using highly trained athletes, we were able to examine changes in complexity of accelerometry over a wide range of running speeds, a range that would not be possible with untrained populations. Still, it is noteworthy that no other investigators have examined changes in complexity during running. Some investigators have applied other non-linear measures such as DFA and/or LyE to running. In particular, Jordan et al. used DFA of stride interval, as well as other gait characteristics, and reported that alpha exhibited a "U-shaped pattern" relative to running speed between 8 and 13 kph with the minima occurring at approximately 10.5 kph, which corresponded to the preferred running speed in this population. These authors have interpreted this data to mean that at speeds corresponding to preferred running speed, constraints are minimal and long range correlations are lost. This is in keeping to a certain extent, although conversely, with our view of CE changes with gait, in that with increasing CE, constraints are reduced, and peak CE would be associated with some least constrained parameters. Running in particular is constrained by an interaction between metabolic power generation, elastic and spring characteristics of the tissues and biomechanical coupling of joints involved in the task [67, 68]. So, although the metabolic cost of running would be least constrained at 8 kph relative to higher speeds in this population, other specific parameters related to the A/P axis may still be relatively unconstrained as speed increases, because peak CE is not observed until later (18 kph) in the A/P axis (Fig 8b).

Changes in Control Entropy at exhaustion

A particularly intriguing aspect of this study was the anticipated CE response at exhaustion, and the stage(s) leading up to it during the running phase of the test. Again, because it has been argued that CE is a measure of system constraint (Bollt et al. 09) and that reduced CE would be indicative of increasing constraints, it was anticipated that at fatigue, or close to it, system constraints would be maximal, and this would be reflected in low, possibly minimal, CE. In keeping with this, in all axes, CE was lower at exhaustion relative to the first running stage (Figures 6b, 7b and 8b). In particular, in both the VERT and M/L axes, CE was lower at exhaustion than even during standing where it might be expected constraints to accelerations of movement would be maximal. In the A/P axis, CE declined throughout the running stages to exhaustion, but CE at exhaustion was approximately equivalent to CE during standing.

Factors contributing to fatigue during maximal running remain elusive [69-72], but LeBris et al. [9] used HRA mounted to the lower back of trained runners in similar fashion to the current study to investigate changes in accelerometion during maximal running bouts. The authors reported that during exhaustive runs at 17 kph, accelerations in the M/L axis increased significantly, while a linear “regularity index” of the VERT axis decreased. LeBris et al. [9] argued that the extra energy expended in the M/L axis as runs progressed contributed to fatigue in these subjects. In the current study, M/L accelerations increased with speed and may have been a contributing factor to fatigue as VO_2 becomes constrained near maximal speeds. In two other studies, Slawinski et al. [3, 70] reported an increase in the internal cost (C_{int})of running during maximal over-ground running to exhaustion, which contrasted a reduction of C_{int} reported by Borrani et al. [71] during treadmill running. The differences in these studies may lie primarily in inherent differences between the two running surfaces. It should be noted though that in one study Slawinski et al. [3] used both fit trained and untrained runners, and reported a difference between the two groups in that the trained runners increased C_{int} to a lesser extent than the untrained runners. This exemplifies the value in using trained runners as subjects in contrast to healthy and diseased comparators as differences can exist between normals and trained individuals of similar fitness, which can then be used to identify potentially abnormal gait parameters in diseased populations.

Likely the most fascinating aspect of this study is the observation of differential complexity responses for individual axes of accelerations collected at the same point in space. This was not anticipated, but may be of value. Because CE is not only a measure of system complexity, but constraint, and moreover the system controller’s effort to maintain a current state of the system, or to respond to a change in state of the system [20], this tool could be of use in clinical situations to identify perturbed control of gait in one component of the system, and more specifically identify pathologies in a

prospective fashion rather than simply identify alterations in gait output such as with stride interval. In general, in contrast to cardiovascular physiology, non-linear measures of variability with respect to gait patterns are associated with diseased states or poor health outcomes [64]. It will be necessary to perform further studies in healthy normal and diseased populations, in contrast to highly trained individuals, under similar experimental conditions to determine if this generalization applies to CE analysis of gait parameters.

Conclusion

The investigation presented here is the first to report changes in the complexity of control constraints in response to increasing speed during both walking and running gaits. Further, this is the first work to take advantage of the properties of CE that enable its application to data collected during exhaustive exercise. Finally, this is the first to examine changes in complexity of gait parameters in walking or running using highly trained athletes as test subjects. This work will serve as a benchmark for comparison against other populations and such comparisons may provide unique insight into the constraints of walking and running. In particular, insights with regard to the constraints of exhaustive running in highly trained runners may provide distinct contrasts to untrained healthy or clinical populations. These differences could be used to identify characteristic constraints in clinical populations and assist in treatment/rehabilitation. Additionally, these distinctions could also be used to determine optimized patterns of complexity that could serve as models for development of robotic locomotor systems.

References

1. Messier SP, Legault C, Schoenlank CR, Newman JJ, Martin DF, Devita P. Risk Factors and Mechanisms of Knee Injuryin Runners. *Med Sci Sports Exerc*. 2008 Oct 8.
2. Davids K, Bennett S, Newell KM. Movement System Variability. Human Kinetics; 2006.
3. Slawinski JS, Billat VL. Difference in mechanical and energy cost between highly, well, and nontrained runners. *Med Sci Sports Exerc*. 2004 Aug;**36**(8):1440-6.
4. Cavanagh P. The mechanics of distance running: a historical perspective. In: Cavanagh, P., editor.
Biomechanics of distance running.: Human Kinetics; 1990.
5. Ferris DP, Sawicki GS, Daley MA. A Physiologist's Perspective on Robotic Exoskeletons for Human Locomotion. *Int J HR*. 2007 Sep;**4**(3):507-28.
6. Gazeau F, Koralsztein JP, Billat V. Biomechanical events in the time to exhaustion at maximum aerobic speed. *Arch Physiol Biochem*. 1997 Oct;**105**(6):583-90.

7. Gerlach KE, White SC, Burton HW, Dorn JM, Leddy JJ, Horvath PJ. Kinetic changes with fatigue and relationship to injury in female runners. *Med Sci Sports Exerc*. 2005 Apr;**37**(4):657-63.
8. Hanon C, Thepaut-Mathieu C, Vandewalle H. Determination of muscular fatigue in elite runners. *Eur J Appl Physiol*. 2005 May;**94**(1-2):118-25.
9. Le Bris R, Billat V, Auvinet B, Chaleil D, Hamard L, Barrey E. Effect of fatigue on stride pattern continuously measured by an accelerometric gait recorder in middle distance runners. *J Sports Med Phys Fitness*. 2006 Jun;**46**(2):227-31.
10. Bogey R, Hornby GT. Gait training strategies utilized in poststroke rehabilitation: are we really making a difference? *Top Stroke Rehabil*. 2007 Nov-Dec;**14**(6):1-8.
11. Bogey RA, Elovic EP, Bryant PR, Geis CC, Moroz A, O'Neill BJ. Rehabilitation of movement disorders. *Arch Phys Med Rehabil*. 2004 Mar;**85**(3 Suppl 1):S41-5.
12. Aziz W, Arif M. Complexity analysis of stride interval time series by threshold dependent symbolic entropy. *Eur J Appl Physiol*. 2006 Sep;**98**(1):30-40.
13. Buzzi UH, Ulrich BD. Dynamic stability of gait cycles as a function of speed and system constraints. *Motor Control*. 2004 Jul;**8**(3):241-54.
14. Georgoulis AD, Moraiti C, Ristanis S, Stergiou N. A novel approach to measure variability in the anterior cruciate ligament deficient knee during walking: the use of the approximate entropy in orthopaedics. *J Clin Monit Comput*. 2006 Feb;**20**(1):11-8.
15. Karmakar CK, Khandoker AH, Begg RK, Palaniswami M, Taylor S. Understanding ageing effects by approximate entropy analysis of gait variability. *Conf Proc IEEE Eng Med Biol Soc*. 2007;**2007**:1965-8.
16. Khandoker AH, Palaniswami M, Begg RK. A comparative study on approximate entropy measure and poincare plot indexes of minimum foot clearance variability in the elderly during walking. *J Neuroeng Rehabil*. 2008;**5**:4.
17. Kurz MJ, Stergiou N. The aging human neuromuscular system expresses less certainty for selecting joint kinematics during gait. *Neurosci Lett*. 2003 Sep 18;**348**(3):155-8.
18. Liao F, Wang J, He P. Multi-resolution entropy analysis of gait symmetry in neurological degenerative diseases and amyotrophic lateral sclerosis. *Med Eng Phys*. 2008 Apr;**30**(3):299-310.
19. Miller DJ, Stergiou N, Kurz MJ. An improved surrogate method for detecting the presence of chaos in gait. *J Biomech*. 2006;**39**(15):2873-6.
20. Bollt EM, Skufca JD, McGregor SJ. Control Entropy: A Complexity Measure for Nonstationary Signals. *Mathematical Biosciences and Engineering*. 2009;**6**(1):1-25.
21. Cavagna G, Saibene F, Margaria R. A three-directional accelerometer for analyzing body movements. *J Appl Physiol*. 1961 Jan;**16**:191.
22. Moe-Nilssen R. A new method for evaluating motor control in gait under real-life environmental conditions. Part 1: The instrument. *Clin Biomech (Bristol, Avon)*. 1998 Jun;**13**(4-5):320-7.
23. Moe-Nilssen R. Test-retest reliability of trunk accelerometry during standing and walking. *Arch Phys Med Rehabil*. 1998 Nov;**79**(11):1377-85.
24. Crouter SE, Churilla JR, Bassett DR, Jr. Estimating energy expenditure using accelerometers. *Eur J Appl Physiol*. 2006 Dec;**98**(6):601-12.

25. Troiano RP. Large-scale applications of accelerometers: new frontiers and new questions. *Med Sci Sports Exerc*. 2007 Sep;**39**(9):1501.
26. Trost SG, Way R, Okely AD. Predictive validity of three ActiGraph energy expenditure equations for children. *Med Sci Sports Exerc*. 2006 Feb;**38**(2):380-7.
27. Ward DS, Evenson KR, Vaughn A, Rodgers AB, Troiano RP. Accelerometer use in physical activity: best practices and research recommendations. *Med Sci Sports Exerc*. 2005 Nov;**37**(11 Suppl):S582-8.
28. McGregor SJ, Busa MA, Yaggie JA, Bollt EM. Using High Resolution MEMS Accelerometers (HRA) for the Estimation of VO2 in Highly Trained Inter-collegiate Distance Runners. *PlosOne*. In review.
29. Moe-Nilssen R. A new method for evaluating motor control in gait under real-life environmental conditions. Part 2: Gait analysis. *Clin Biomech (Bristol, Avon)*. 1998 Jun;**13**(4-5):328-35.
30. Eckmann JP, Ruelle D. Ergodic theory of chaos and strange attractors. *Rev Mod Phys*. 1985;**57**(2):617-56.
31. Takens F, et al. Detecting strange attractors in turbulence. *Lecture Notes in Mathematics*. 1981;**898**(1):366-81.
32. Ott E, Sauer T, Yorke JA. Coping with chaos. Analysis of chaotic data and the exploitation of chaotic systems. New York: John Wiley; 1994.
33. Sirovich L. Chaotic dynamics of coherent structures. *Physica D*. 1989;**37**:126-45.
34. Cover TM, Thomas JA. Elements of Information Theory. New York: Wiley-Interscience New York; 2006.
35. Shannon CE, Weaver W. The Mathematical Theory of Information. Urbana: University of Ilinois Press; 1949.
36. Renyi A. On measures of entropy and information. *Proceedings of the 4th Berkeley Symposium on Mathematical Statistics and Probability*. 1961;**1**:547-61.
37. Grassberger P, Procaccia I. Estimation of the Kolmogorov entropy from a chaotic signal. *Physical Review A*. 1983;**28**(4):2591-3.
38. Zyczkowski K. Renyi Extrapolation of Shannon Entropy. *Open Systems & Information Dynamics*. 2003;**10**(3):297-310.
39. Kantz H, Schreiber T. Nonlinear Time Series Analysis. Cambridge: Cambridge University Press; 2004.
40. Pincus SM. Approximate Entropy as a Measure of System Complexity. *Proceedings of the National Academy of Sciences of the United States of America*. 1991;**88**(6):2297-301.
41. Pincus SM. Assessing Serial Irregularity and Its Implications for Health. *Annals of the New York Academy of Sciences*. 2001;**954**(1):245.
42. Pincus SM, Goldberger AL. Physiological time-series analysis: what does regularity quantify? *American Journal of Physiology- Heart and Circulatory Physiology*. 1994;**266**(4):1643-56.
43. Bollt E, Stanford T, Lai Y-C, Zyczkowski K. Validity of threshold-crossing analysis of symbolic dynamics from chaotic time series. *Physical Review Letters*. 2000;**85** (16):3524-7.

44. Bollt E, Stanford T, Lai Y-C, Zyczkowski K. What Symbolic Dynamics Do We Get With A Misplaced Partition? On the Validity of Threshold Crossings Analysis of Chaotic Time-Series. *Physica D*. 2001;**154** (3-4):259-86.
45. Lin J, Keogh E, Lonardi S, Chiu B. A symbolic representation of time series, with implications for streaming algorithms. *Proceedings of the 8th ACM SIGMOD workshop on Research issues in data mining and knowledge discovery*. 2003:2-11.
46. Holmes P, Lumley JL, Berkooz G. Turbulence, Coherent Structures, Dynamical Systems and Symmetry. 1996.
47. Golub GH, Van Loan CF. Matrix Computations The Johns Hopkins University Press; 1996.
48. Sirovich L, Kirby M. Low-dimensional procedure for the characterization of human faces. *Journal of the Optical Society of America*. 1987;**A4**:519-24.
49. Press WH, Flannery BP, Teukolsky SA, Vetterling WT. Numerical Recipes in C: The Art of Scientific Computing. 2 ed.: Cambridge University Press; 1992.
50. Draper NR, Smith H. Applied Regression Analysis, . 2 ed. New York: John Wiley; 1981.
51. Chang YH, Huang HW, Hamerski CM, Kram R. The independent effects of gravity and inertia on running mechanics. *J Exp Biol*. 2000 Jan;**203**(Pt 2):229-38.
52. Chang YH, Kram R. Metabolic cost of generating horizontal forces during human running. *J Appl Physiol*. 1999 May;**86**(5):1657-62.
53. Glazier PS, Davids K. Constraints on the complete optimization of human motion. *Sports Med*. 2009;**39**(1):15-28.
54. Joyner MJ, Coyle EF. Endurance exercise performance: the physiology of champions. *J Physiol*. 2008 Jan 1;**586**(1):35-44.
55. Coyle EF. Physiological determinants of endurance exercise performance. *J Sci Med Sport*. 1999 Oct;**2**(3):181-9.
56. Howlett RA, Kirkton SD, Gonzalez NC, Wagner HE, Britton SL, Koch LG, et al. Peripheral oxygen transport and utilization in rats following continued selective breeding for endurance running capacity. *J Appl Physiol*. 2008 Apr 17.
57. Noland RC, Thyfault JP, Henes ST, Whitfield BR, Woodlief TL, Evans JR, et al. Artificial selection for high-capacity endurance running is protective against high-fat diet-induced insulin resistance. *Am J Physiol Endocrinol Metab*. 2007 Jul;**293**(1):E31-41.
58. Britton SL, Koch LG. Animal models of complex diseases: an initial strategy. *IUBMB Life*. 2005 Sep;**57**(9):631-8.
59. Daniels JT. A physiologist's view of running economy. *Med Sci Sports Exerc*. 1985 Jun;**17**(3):332-8.
60. Foster C, Lucia A. Running economy : the forgotten factor in elite performance. *Sports Med*. 2007;**37**(4-5):316-9.
61. Lucia A, Esteve-Lanao J, Olivan J, Gomez-Gallego F, San Juan AF, Santiago C, et al. Physiological characteristics of the best Eritrean runners-exceptional running economy. *Appl Physiol Nutr Metab*. 2006 Oct;**31**(5):530-40.
62. Lucia A, Olivan J, Bravo J, Gonzalez-Freire M, Foster C. The key to top-level endurance running performance: a unique example. *Br J Sports Med*. 2008 Mar;**42**(3):172-4; discussion 4.

63. Nummela AT, Paavolainen LM, Sharwood KA, Lambert MI, Noakes TD, Rusko HK. Neuromuscular factors determining 5 km running performance and running economy in well-trained athletes. *Eur J Appl Physiol*. 2006 May;**97**(1):1-8.
64. Hausdorff JM. Gait dynamics, fractals and falls: finding meaning in the stride-to-stride fluctuations of human walking. *Hum Mov Sci*. 2007 Aug;**26**(4):555-89.
65. Neptune RR, Sasaki K, Kautz SA. The effect of walking speed on muscle function and mechanical energetics. *Gait Posture*. 2008 Jul;**28**(1):135-43.
66. England SA, Granata KP. The influence of gait speed on local dynamic stability of walking. *Gait Posture*. 2007 Feb;**25**(2):172-8.
67. Saibene F, Minetti AE. Biomechanical and physiological aspects of legged locomotion in humans. *Eur J Appl Physiol*. 2003 Jan;**88**(4-5):297-316.
68. Sasaki K, Neptune RR. Muscle mechanical work and elastic energy utilization during walking and running near the preferred gait transition speed. *Gait Posture*. 2006 Apr;**23**(3):383-90.
69. Slawinski J, Heubert R, Quievre J, Billat V, Hannon C. Changes in spring-mass model parameters and energy cost during track running to exhaustion. *J Strength Cond Res*. 2008 May;**22**(3):930-6.
70. Slawinski JS, Billat VL. Changes in internal mechanical cost during overground running to exhaustion. *Med Sci Sports Exerc*. 2005 Jul;**37**(7):1180-6.
71. Borrani F, Candau R, Perrey S, Millet GY, Millet GP, Rouillon JD. Does the mechanical work in running change during the VO2 slow component? *Med Sci Sports Exerc*. 2003 Jan;**35**(1):50-7.
72. Candau R, Belli A, Millet GY, Georges D, Barbier B, Rouillon JD. Energy cost and running mechanics during a treadmill run to voluntary exhaustion in humans. *Eur J Appl Physiol Occup Physiol*. 1998 May;**77**(6):479-85.

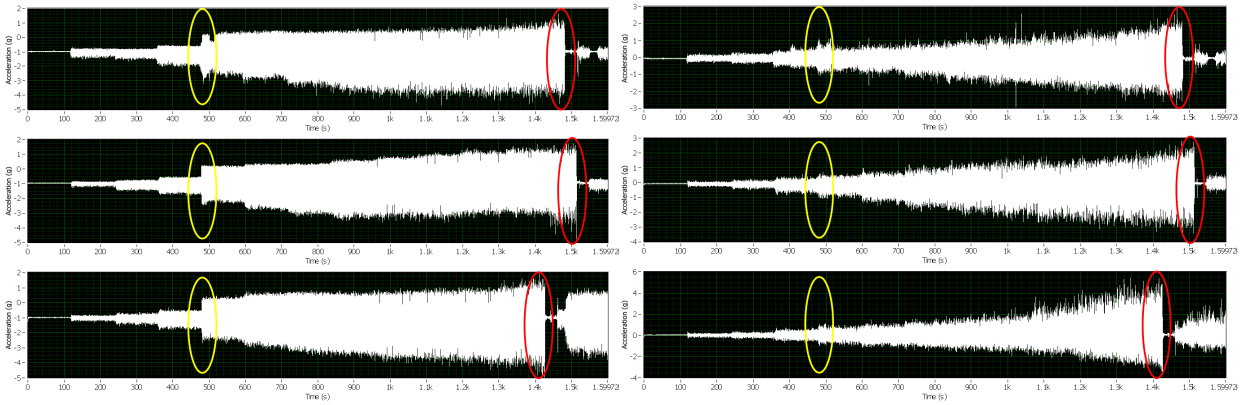
Acceleration (g)
Time (s)

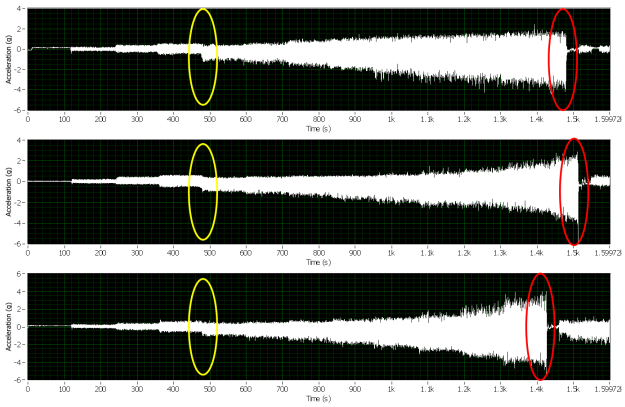
Acceleration (g)
Time (s)

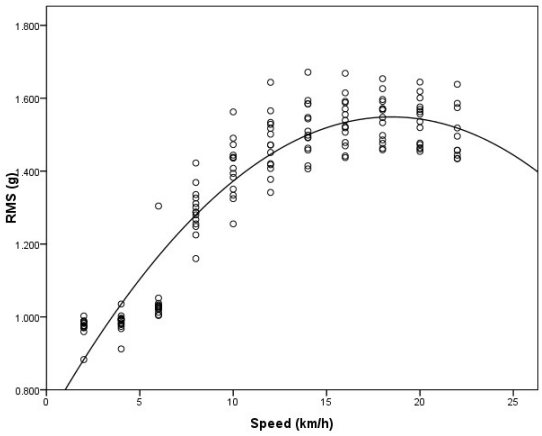
RMS (g)
Speed (km/h)

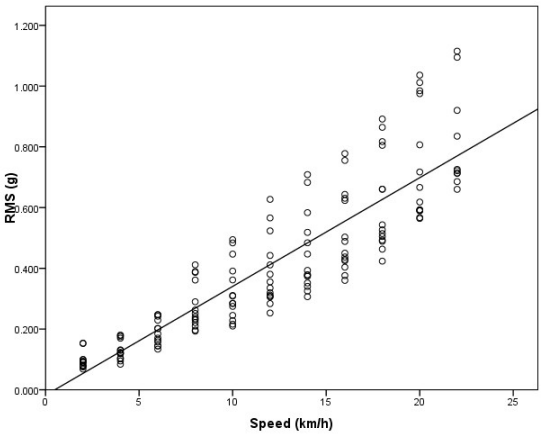
RMS (g)
Speed (km/h)

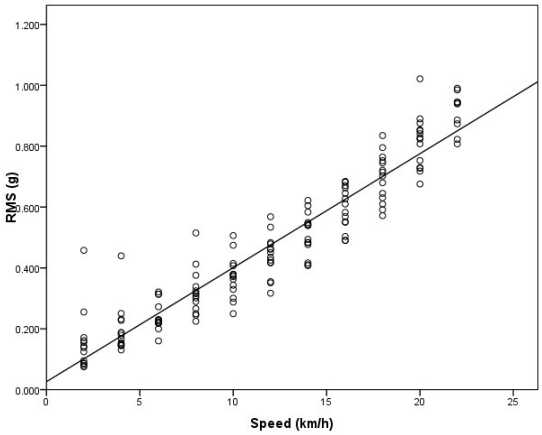
RMS (g)
Speed (km/h)

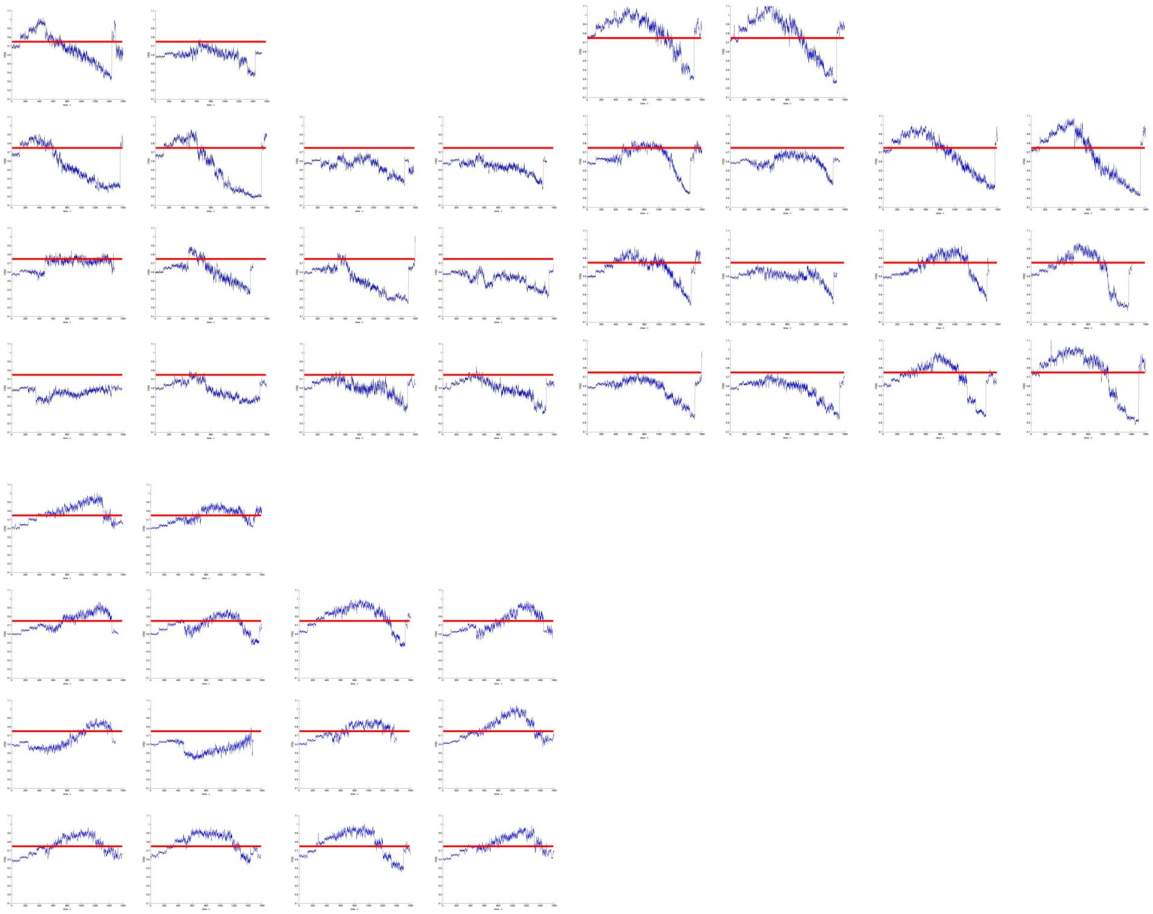

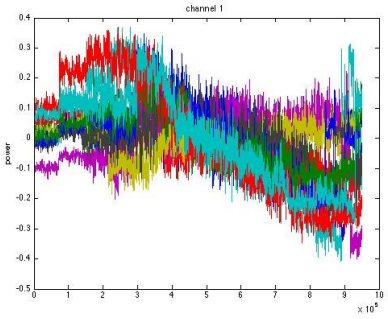
channel 1
power
x 10^5

a)

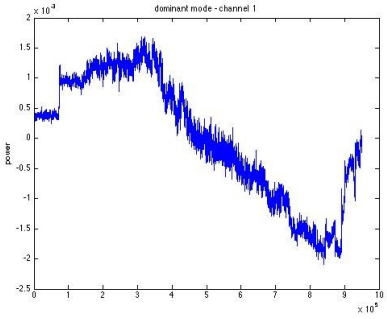
dominant mode - channel 1
x 10^-3
power
x 10^5

b)

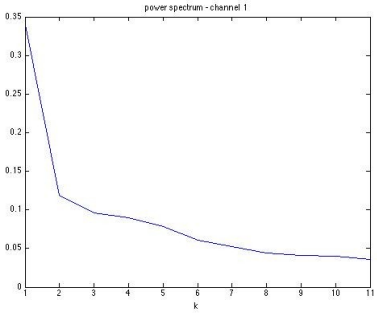
power spectrum - channel 1
k

c)

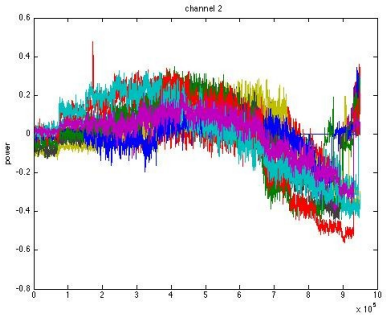
channel 2
power
x 10^5

a)

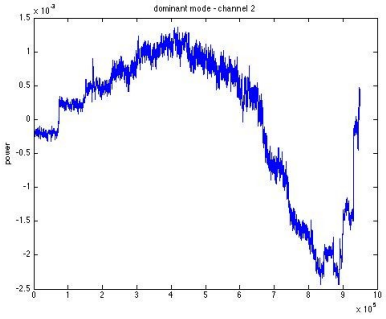
dominant mode - channel 2
x 10^-3
power
x 10^5

b)

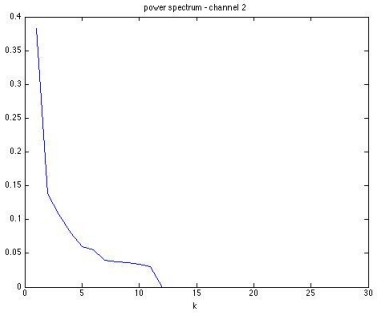
power spectrum - channel 2
k

c)

a)

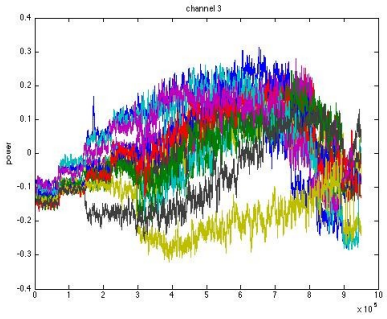
channel 3
power
x 10^5

b)

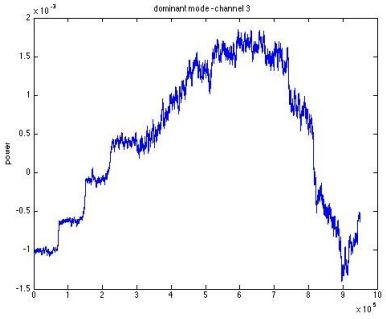
dominant mode - channel 3
power
x 10^-3
x 10^5

c)

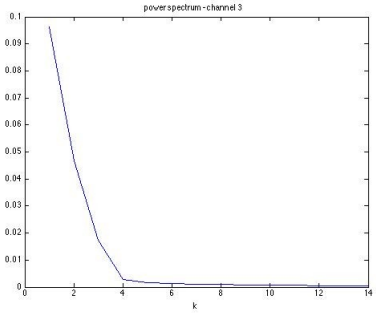
power spectrum - channel 3
k

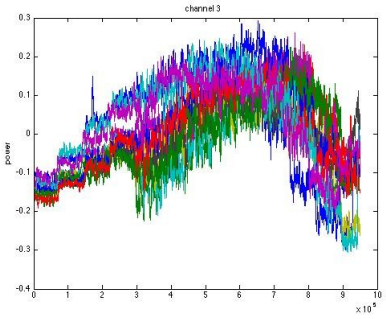
channel 3
power
0.3
0.2
0.1
0
-0.1
-0.2
-0.3
-0.4
0 1 2 3 4 5 6 7 8 9 10
x 10^5

a)

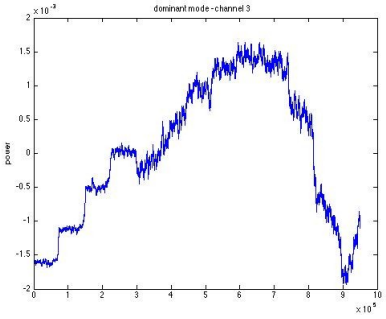
dominant mode - channel 3
x 10^-3
power
2
1.5
1
0.5
0
-0.5
-1
-1.5
-2
0 1 2 3 4 5 6 7 8 9 10
x 10^5

b)

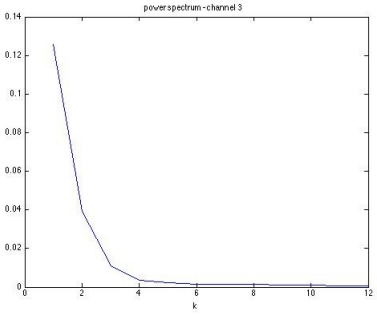
power spectrum - channel 3
0.14
0.12
0.1
0.08
0.06
0.04
0.02
0
0 2 4 6 8 10 12
k

c)

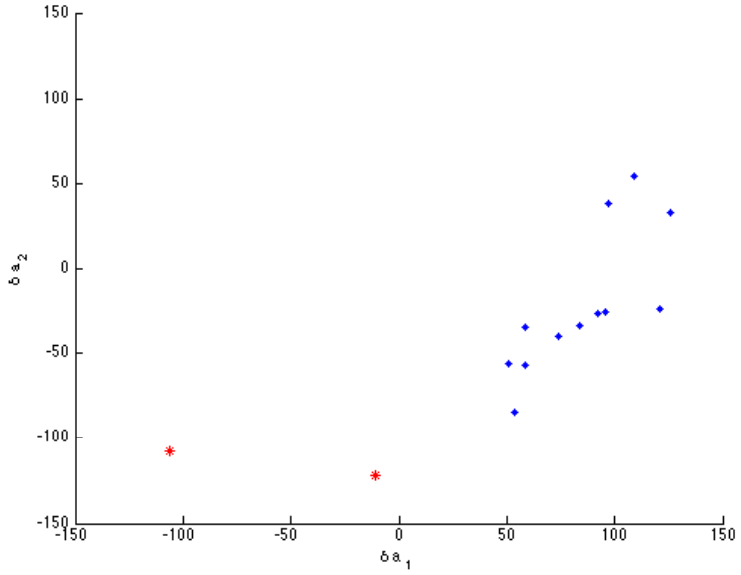
150
100
50
0
-50
-100
-150
δa2
-150
-100
-50
0
50
100
150
δa1